Journal of King Saud University – Science 32 (2020) 2445–2453

Contents lists available at ScienceDirect

Journal of King Saud University – Science

journal homepage: www.sciencedirect.com

Original article

Engineering bedrock depth estimation and ground response analysis of the northern Jeddah urban area, western Saudi Arabia

Saad Mogren

Geology and Geophysics Department, King Saud University, Riyadh, Saudi Arabia

ARTICLE INFO

Article history:
Received 8 October 2019
Revised 11 March 2020
Accepted 19 March 2020
Available online 1 April 2020

Keywords:
Bedrock
Ground response
Spectral acceleration
Jeddah
Saudi Arabia

ABSTRACT

The engineering bedrock depth was determined in the northern Jeddah urban area via multichannel analysis of surface waves (MASW) conducted at 76 locations. Depths corresponding to the velocity ranges were estimated below the ground surface and mapped. The engineering bedrock depth was evaluated and it varies from 0 to approximately 36.23 m whereas the depth increased eastward. Further, ground response analysis was conducted to assess the seismic hazard in terms of peak ground acceleration, where it ranges from 3.37 to 17.71 cm/s^2, considering the fundamental resonance frequency and amplification potential at the sites of measurement. These variations are due to differences in the soil profile at each location; ground surface acceleration increased at sites with thick layers of soft sediments. In addition, the spectral acceleration and response spectra were assessed at the ground surface with a 5% damping ratio for the identified lithological units. Peak spectral acceleration varies from 16.8 to 62.6 cm/s^2. The eastern zone has a higher spectral acceleration than the western zone while the frequency corresponding to the spectral acceleration varies from 1.05 to 14.28 Hz. The spectral acceleration and response spectra are used for assessment the spectrum of structures. Ground response analysis shows that because of the soil condition, potential amplification of wave amplitudes is observed at the ground surface when compared to the engineering bedrock level acceleration. These results should be provided to civil engineers, land-used planners, and decision makers during the designing of either new buildings or rehabilitation of pre-existing structures.

1. Introduction

The evaluation of the spatial changeability of the engineering bedrock depth in urban expansion zones using multichannel analysis of surface waves (MASW) survey is important for various applications to allocate the input parameters for response spectra. Through geotechnical investigations, the bedrock identification has great importance to adopt the kind of foundation for appropriate structure. Both of peak ground acceleration (PGA) and spectra at a particular site are evaluated for bedrock and ground surface levels including local site response effects. The main objective of our work is the engineering bedrock depth estimation for northern Jeddah area based on shear-wave velocity, V_s, measured through MASW survey. MASW becomes a widespread seismic method applied for geotechnical classification of shallow sediments (Miller et al., 1999; Park et al., 1999; Xia et al., 1999; Park and Miller, 2005; Kanli et al., 2006; Kanlı, 2010; Rehman et al., 2016). Furthermore, MASW is more efficient for determining shallow subsurface properties (Park et al., 2001; Zhang et al., 2004). Aldahri et al. (2017) conducted site soil classification for surface soil in Ubhur area according to the national earthquake hazards reduction program (NHREP) recommendations where, the greatest part of the study area falls in site class C while class B and D covered limited areas in the western and the eastern parts respectively.

The results of MASW include vertical and cross-section of vs profiles. MASW was applied through the study area for 76 sites for shear wave velocity assessment. The estimated values were analyzed and then the engineering bedrock surface depth was classified. The engineering bedrock can be defined as the layer having shear-wave velocity about 700 m/s (Miller et al., 1999; Santamarina et al., 2001; Ryden, 2004; Nath, 2007). While Ansal and Tonuk (2007) indicate that the bedrock layers have Vs varying

Peer review under responsibility of King Saud University.

Production and hosting by Elsevier

E-mail address: smogren@ksu.edu.sa

https://doi.org/10.1016/j.jksus.2020.03.037
1018-3647/

from 700 to 750 m/s. moreover the program NEHRP (2009) and (Akin et al., 2013), illustrated the value of 760 m/s corresponds to the bedrock.

Depending on the majority of studies, the depth equivalent to Vs of 760 m/s is taken as the engineering bedrock depth in this study. Then, the identified bedrock depths have been mapped illustrating the engineering bedrock depth surface in the northern Jeddah urban area.

2. Study area and local geology

The studied area lies sideways the Red Sea coast to the north of Jeddah city, west Saudi Arabia (Fig. 1). The study area is the northern expansion part of Jeddah area, which has been subject to moderate earthquakes (Fnais et al., 2010). Some of these earthquakes have been felt through the Jeddah region. The maximum moment magnitude (M_w) was 7.2 in 1967 occurred through the Red Sea axial trough and affected the study area (Ambraseys et al., 1994). Unfortunately, the surface soil of the study area ranges from very soft to massive/stiff sediments or rocks. Some of sediments have poor geotechnical properties (e.g., the sabkhah deposits) and consequently cause the damages of buildings and structures in the case of strong earthquakes.

The surface geology of northern Jeddah was evaluated by Moore and Al-Rehaili (1989) and differentiated as follows (Fig. 2): Ubhur Formation of early Miocene which consists of green siltstone, and limestone. These Tertiary units have been tilted and overlain northward by alkaline basalt of the Miocene to Pliocene Rahat

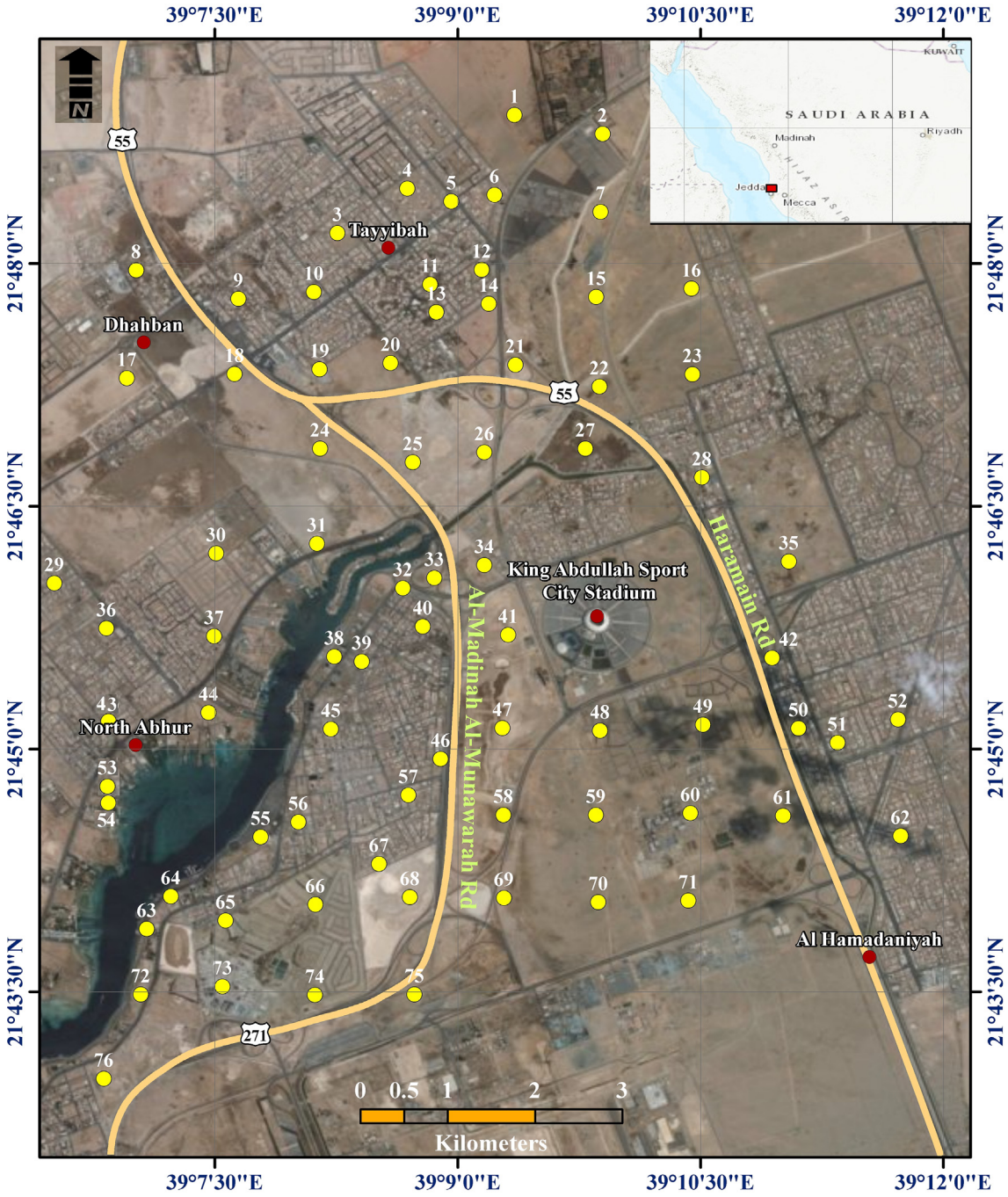

Fig. 1. Location map of the study area (Yellow circles are the locations of MASW sites).

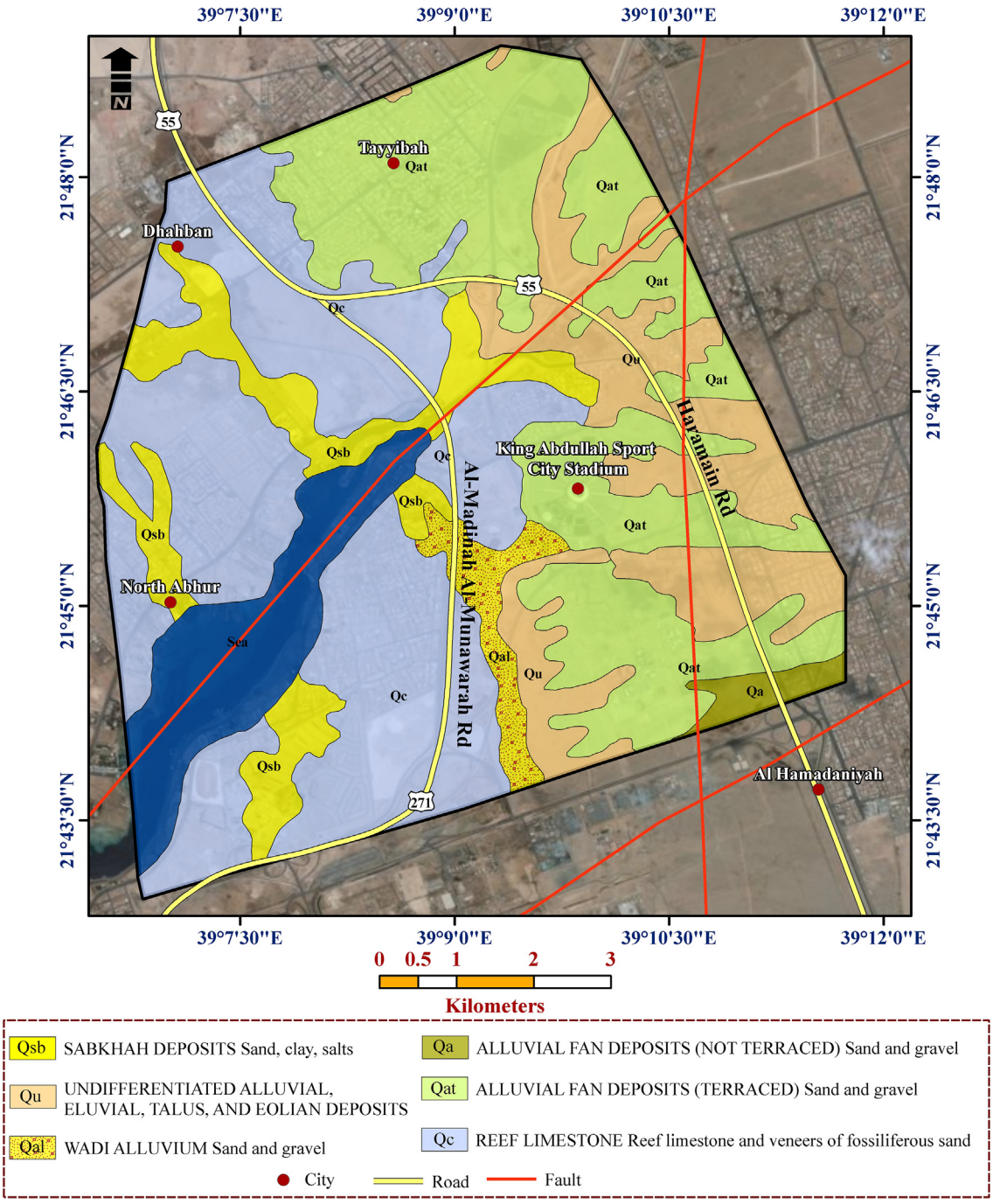

Fig. 2. Geological map for the study area.

Group. The Quaternary deposits have been divided into seven lithological units. The oldest is a raised reef limestone that outcrops in the western part followed by undifferentiated alluvial, eolian, and sabkha deposits, which are the youngest. These alluvial fan deposits are divided into two types: terraced and non-terraced deposits. The terraced deposits are composed of poorly sorted, coarse-grained gravels and beds containing a high proportion of cobbles and boulders. The other type is composed of gravel and sand. The reef limestone is widespread westward and raised 3–6 m above sea level and not exposed because it is covered sabkha. Moreover, there are small sabkha deposits detached westward.

3. Data acquisition and processing

3.1. Engineering bedrock depth estimation

MASW field data in this study were acquired using Geode seismograph equipped by 24 vertical geophones with 4.5-Hz. Seismic waves were produced by an impulsive source of weight drop. The recorded waves were analyzed using the SurfSeis software to produce a 1-D or 2-D Vs data through three processing steps as follows: i) field-data preparation, ii) dispersion-curve construction, and finally, iii) inversion process. The selected sites for MASW are distributed throughout the study area and cover the identified

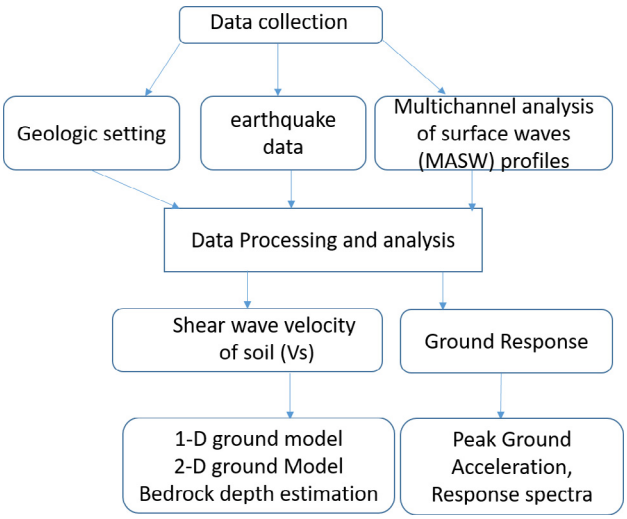

Fig. 3. Flowchart showing the methodologies applied in this study.

geologic units. Seventy-six of 1-D MASW surveying profiles were conducted in the investigated area. Field data were collected with 1-m geophone spacing. The energy source was sustained at a distance of 10 m. This source distance is recommended for recording high quality signals within very soft, soft, and hard soils. Then, shear-wave velocity model was assessed through the inversion process based on least-squares fitting algorithm (Xia et al., 1999).

The engineering bedrock depth were estimated for each site of one dimensional velocity profiles of the MASW measurements and the corresponding Vs values (Figs. 3 and 4). Then, shear wave velocity represents the key for calculating seismic hazard at a certain site where the average shear wave velocity for the depth "d" of soil is referred as V_H as follows; the average shear wave velocity up to a depth of H (V_H) is computed according to Kanli et al. (2006) as;

$$V_H = \sum d_i / \sum (d_i / v_i)$$

where H = $\sum d_i$ = Cumulative depth in meters.

For 30 m average depth, shear wave velocity is written as (Boore, 2004):

$$V_{s(30)} = \frac{30}{\sum_{i=1}^{N} (d_i / v_i)}$$

where d_i and v_i denote the thickness (in meters) and shear-wave velocity in *m/s* of the *ith* layer, respectively.

The estimated engineering bedrock depth is shown in Fig. 4. Notably, the corresponding velocity of the overlying soil spans from 200 to 752.05 m/s down to the engineering bedrock level. The average Vs values ranges from 200 to 400 m/s, which can be categorized as medium to dense soil. Whereas the engineering bedrock depth varies between 0 and 36.2 m.

3.2. Ground response assessment

Ground response analyses were applied to calculate surface ground motions by assessing the potential amplification that is used to construct the design response spectrum. In this study due to the lack of acceleration records of any earthquake, it was essential to use the synthetic seismogram. The synthetic ground motion was developed using Boore's *SMSIM* program (Boore, 1983; 2003) at the 76 MASW sites and then, applied for ground response analysis.

The Fourier amplitude spectrum of the ground motion at a site is written as follows:

$$Y(M_0, R, f) = E(M_0, f)\, P(R, f) G(f) I(f)$$

where M_0 is the seismic moment and can be estimated using the following equation (Hanks and Kanamori, 1979);

$$M = \frac{2}{3} \log M_0 - 10.7$$

The source spectra for all of the models can be given by;

$$E(M_0, f) = C M_0 S(M_0, f)$$

where C is a constant, given below, and S (M0, f) is the displacement source spectrum, given by the equation $C = R\theta\varphi FH / 4\pi\sigma\beta^3 r$, and

$$S(M_0, f) = S_a(M_0, f) \times S_b(M_0, f)$$

where, $^{R}\theta\phi$ represents the radiation pattern for a range of azimuths θ and takeoff angles ϕ. F accounts for the free surface effect. H is the reduction factor that accounts for the partitioning of energy into two horizontal components and r is the hypocentral distance, σ and β are crustal density and shear wave velocity. Input parameters for the stochastic model are shown in Table 1 according to Sokolov and Zahran (2018).

The source spectrum was calculated as follows (Brune, 1970);

$$\text{Source}\,(f) = M_o / (1 + (f/fc)^2$$

where M_o is the seismic moment and f_c is corner frequency, respectively.

The value of f_c is acquired by

$$fc = 4.9 \times 10^6 \beta (\Delta\sigma / Mo)^{1/3}$$

where, f_c, β, $\Delta\sigma$ (stress drop), and M_o are in Hertz, km/s, bars and dyne-cm, respectively.

The path spectrum can be calculated depending on both of the geometrical spreading and quality factor Q(f) as given below,

$$\text{Path}\,(f) = GSP(r) \exp(-\pi f r / Q(f) \beta)$$

While, site spectrum can be interpreted as function of frequency dependent amplification A (f) and diminution D (f) factors as,

$$\text{Site}\,(f) = A(f) \times D(f)$$

The amplification of waves as they travel upward to the surface through a rock column is given by

$$A(f) = \{\rho \times \beta / \rho(z) avg \times \beta avg(z)\}^{1/2}$$

$\rho\,(z)_{avg}$ and $\beta_{avg}(z)$ are averages of near-surface density and velocity from the surface to the depth of a quarter wavelength (Boore and Joyner, 1997).

The diminution factor D (f) is given by the following equation

$$D(f) = \exp(-\pi kof)$$

where, k_0, is the distance-independent high frequency attenuation operator (Kappa factor).

Type (f) is a filter used to shape the spectrum corresponding to the particular ground motion and is given by

$$\text{Type}\,(f) = (2\pi f)^s$$

where, s = 0 for acceleration, 1 for velocity, and 2 for displacement

The distinctive synthetic ground motion at the bedrock throughout peak ground acceleration (PGA) is the most commonly used for ground response measurement at a particular site.

In this study, the peak acceleration at the ground surface for each location was assessed depending on the estimated resonance frequency (f_0) and amplification factor (A_0) at each site of MASW measurements (Aldahri et al., 2018). The results of the ground response analysis were mapped using the ArcGIS 9.2 package. The PGA at the ground surface for all MASW sites was estimated.

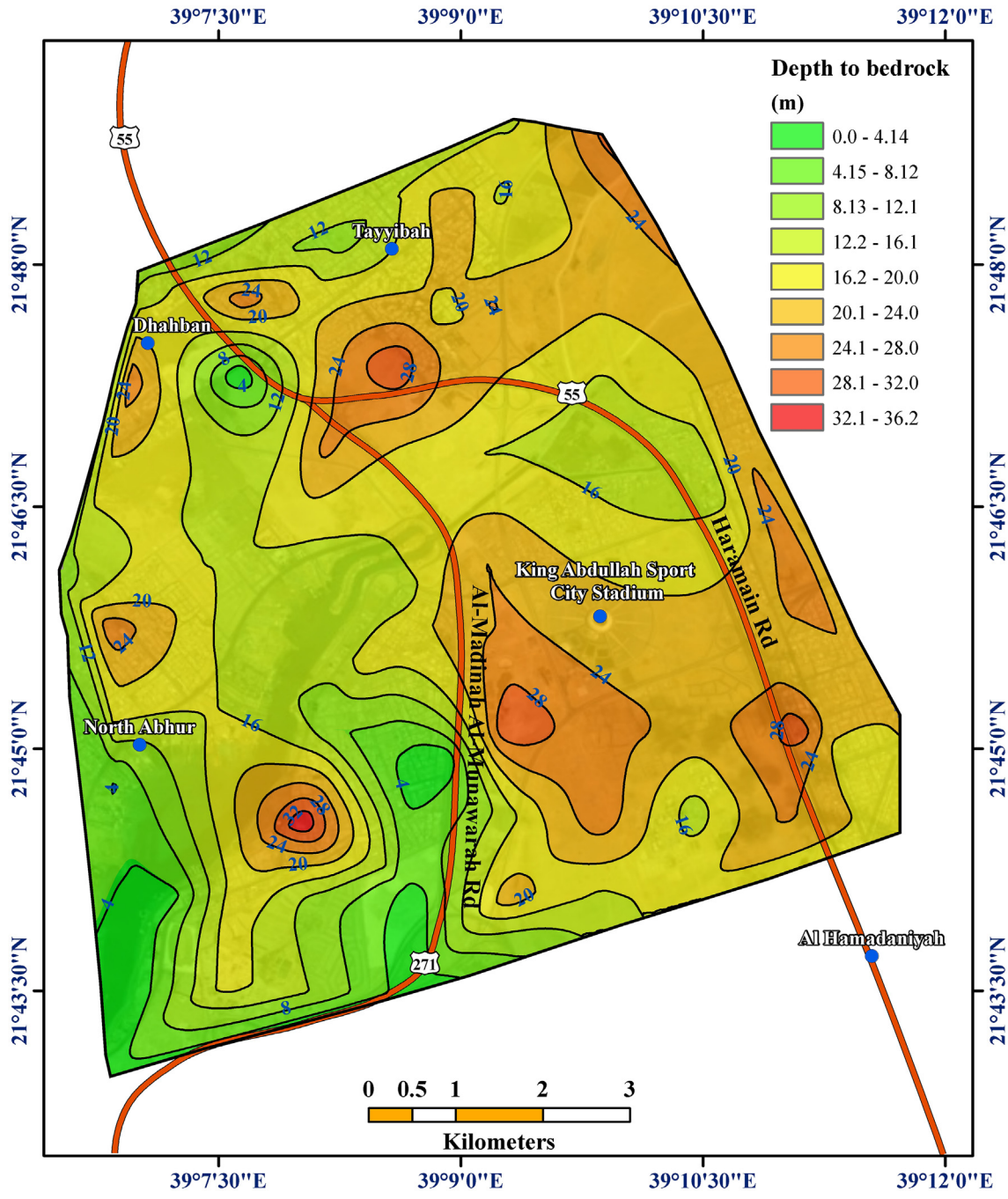

Fig. 4. Depth to the engineering bedrock in the study area.

Table 1
Input parameters for the western Saudi Arabia stochastic model (Sokolov and Zahran, 2018).

Factor	Parameter	Representative value
Source	Slip distribution	Random slip
	Stress drop $\Delta\sigma$	15 bars (1.5 Mpa)-90 bars (9 Mpa)
	Shear-wave velocity β	3.0 km/s
	Density ρ	2.8 g/cm^3
	Rupture propagation velocity	0.8 β
Path	Geometric spreading	Trilinear, R^{-1} for R < 40 km; R^0 for 40 $\leq$ R < 70 km; $R^{-0.5}$ for R $\geq$ 70 km
	Quality factor	$Q(f) = 250\, f^{0.6}$
	Duration	$1/f_c + 0.05\, R_{Hypo}$
Site	kappa-effect	0.02 and 0.04s

Table 2 shows the variation in the *PGA* value from 3.37 to 17.71 cm/s^2. These variations in the ground surface PGA values are based on the variations in the soil profile at each location, where the ground surface acceleration increases at sites with thick soft sediment layers. The ground surface acceleration is considerably higher in areas of alluvial deposits as a result of the thick silty sand layers. Depending on the PGA values at the bedrock and ground surface, it is clear that the *PGA* at the bedrock surface is influenced by the distance, while local site response effects influence the PGA at the ground surface.

4. Results and discussion

The estimated shear-wave velocity at 76 MASW locations used to identify the engineering bedrock depth at each site (Fig. 4). The

Table 2
Results of ground response analysis at the study area.

Site No.	Lat.	Long.	F_0	A_0	PGA (bedrock)	PGA (surface)	PGA (1.5 Hz)	PGA (3 Hz)	PGA (5 Hz)	PGA (8 Hz)	PGA (10 Hz)	Max. PSA	Max. Hz
1	21.81528	39.15585	2	2.06	6.44	8.26	16.46	11.48	12.47	15.38	16.22	17.43	14.286
2	21.81333	39.16494	5.402	4.4	6.44	17.77	35.71	42.18	39.09	23.95	24.12	45.18	4.167
3	21.8031	39.13762	1.361	1.59	5.13	7.146	11.19	10.78	11.89	15.02	16.08	16.82	13.333
4	21.80768	39.14483	1.361	2.15	4.8	8.018	14.41	11.19	12.51	15.75	16.66	17.38	13.333
5	21.80637	39.14935	1.522	2.35	4.8	8.487	17.28	11.63	12.9	16.07	16.96	17.63	13.333
6	21.80705	39.15381	1.848	1.81	4.58	7.624	14.33	10.83	12.23	15.41	16.41	17.07	13.333
7	21.8053	39.16472	4.138	3.31	4.71	13.02	26.74	31.39	19.44	19.58	20.3	32.77	3.571
8	21.79929	39.1169	1.202	2.87	6.75	9.354	16.45	12.72	13.31	16.69	17.56	19.98	1.176
9	21.79635	39.12744	1.991	2.08	6.75	8.377	16.68	12.01	12.63	16.1	16.85	17.63	13.333
10	21.79704	39.1352	1.43	1.69	6.71	7.402	12.4	11.13	11.87	15.49	16.3	17.11	13.333
11	21.79783	39.14718	1.38	1.37	5.3	6.893	10.29	10.63	11.5	15.16	15.97	16.83	13.333
12	21.79933	39.15248	1.64	2.2	5.13	8.406	16.92	11.96	12.85	15.86	16.84	17.54	12.5
13	21.79497	39.14782	1.31	1.34	6.52	6.829	9.919	10.58	11.43	15.07	15.98	16.8	13.333
14	21.79584	39.15322	1.472	2.65	5.29	9.217	18.64	12.74	13.39	16.4	17.38	19.46	1.25
15	21.79652	39.16427	2.07	2.58	5.13	9.511	20.4	13.07	13.72	16.65	17.53	20.76	1.667
16	21.79738	39.17408	5.746	5.93	4.97	23.93	47.14	57.38	63.51	31.38	30.7	63.61	5
17	21.78816	39.11595	1.306	3.68	5.48	11.17	21.84	13.95	14.93	17.55	18.74	26.72	1.176
18	21.7886	39.12703	1.991	2.06	6.28	8.258	16.74	11.63	12.78	15.81	16.95	17.84	13.333
19	21.78908	39.13578	1.491	1.65	6.28	7.263	12.71	10.59	11.99	15.22	16.34	17.3	13.333
20	21.78972	39.1431	4.03	1.486	6.96	7.543	12.21	14.5	12.6	15.61	16.39	17.26	13.333
21	21.78954	39.15597	1.448	2.69	6.75	9.253	18.8	12.7	13.28	16.65	17.49	19.45	1.333
22	21.7873	39.16461	2.01	3.01	6.67	10.47	24.2	13.98	14.28	17.51	18.27	24.44	1.667
23	21.78857	39.17419	3.47	3.25	6.52	12.64	26.24	31.26	17.3	19.15	20.25	31.38	2.941
24	21.78092	39.13583	1.17	2.55	4.78	8.834	15.07	11.85	13.07	16.03	17.14	18.34	1.176
25	21.77952	39.14538	1.387	1.75	4.98	7.478	12.76	10.75	12.09	15.26	16.36	17.44	13.333
26	21.78053	39.15276	5.08	3.378	5.65	14.08	27.86	33.25	31.91	20.75	21.46	34.78	4.545
27	21.78091	39.16315	1.7	2.4	6.42	8.864	19.13	12.09	13.2	16.14	17.31	19.13	1.5
28	21.77794	39.17516	1.87	2.73	6.42	9.965	22	12.93	13.87	16.68	17.85	22	1.5
29	21.76705	39.10847	1.19	2.58	5.48	9.096	14.88	12.11	13.52	16.69	17.52	18.61	14.286
30	21.77012	39.12514	1.435	3.41	5.85	10.87	22.86	13.97	14.88	17.67	18.57	25.12	1.25
31	21.77113	39.13552	1.296	5.95	5.87	15.97	31.66	18.51	19.44	21.78	22.41	43.32	1.176
32	21.76653	39.14437	1.183	2.26	5.88	8.358	13.8	11.62	12.98	15.91	16.98	18.04	13.333
33	21.7676	39.1476	1.157	2.12	5.87	8.15	13.15	11.34	12.81	15.72	16.77	18	12.5
34	21.76892	39.15275	1.379	1.99	5.83	8.107	14.15	11.17	12.69	15.64	16.68	17.95	12.5
35	21.7693	39.18411	1.256	2.86	4.78	9.511	17.29	12.46	13.61	16.46	17.58	21.04	1.176
36	21.76242	39.11384	1.107	3.66	6.1	11.01	18.01	13.6	15.18	18.28	18.8	24.99	1.053
37	21.76162	39.12493	1.46	3.52	5.96	11.33	23.72	14.13	15.5	18.47	19.1	26.2	1.333
38	21.75951	39.13731	1.461	3.01	5.84	10.25	20.62	13.17	14.56	17.58	18.31	22.47	1.333
39	21.75899	39.14012	1.41	3.22	2.74	10.63	20.92	13.49	14.87	17.87	18.57	23.77	1.333
40	21.76261	39.14641	1.324	2.119	5.54	8.155	13.97	11.49	12.79	15.84	16.96	17.94	13.333
41	21.76174	39.15519	1.513	2.374	5.54	8.784	17.38	12.1	13.25	16.23	16.44	18.32	13.333
42	21.75936	39.18238	1.069	2.825	5.87	9.269	15.15	12.29	13.68	16.48	17.44	18.96	1.053
43	21.75284	39.11405	0.992	4.25	6.27	11.87	18.85	14.64	15.75	18.43	19.57	27.38	1
44	21.75374	39.12434	1.203	2.381	6.32	8.806	14.21	11.83	13.36	16.41	17.4	18.45	13.333
45	21.75204	39.13694	1.76	2.16	6.23	8.759	16.84	11.89	13.34	16.41	17.34	18.37	13.333
46	21.74895	39.14825	1.409	2.347	6.23	8.904	16	11.92	13.44	16.53	17.4	18.48	13.333
47	21.75215	39.15461	1.35	2.04	6.11	8.221	13.7	11.32	13.01	16.28	16.96	18.03	14.286
48	21.75187	39.16466	1.209	2.259	5.96	8.522	13.68	11.59	13.19	16.38	17.18	18.26	14.286
49	21.75249	39.17526	1.256	5.09	5.42	14.08	26.1	16.77	17.66	20.59	21.16	35.69	1.176
50	21.75211	39.18511	1.067	2.49	5.45	8.653	13.54	11.83	13.06	16.29	17.23	18.21	14.286
51	21.75062	39.18912	1.506	3.06	5.45	10.28	21.65	13.36	14.34	17.35	18.24	22.65	1.429
52	21.75304	39.19536	1.94	3.06	5.85	10.74	24.55	14.15	14.76	17.5	18.48	24.79	1.667
53	21.74611	39.1141	1.102	2.06	4.95	8.119	12.66	11.36	12.75	15.77	17.07	18.34	13.333
54	21.74442	39.11402	1.028	3.36	4.97	10.42	16.74	13.25	14.46	17.37	18.41	22.12	1.053
55	21.74092	39.12971	1.166	3.71	4.97	11.25	19.02	14.05	15.16	17.98	19.01	25.72	1.111
56	21.74247	39.1336	1.256	4.79	5.16	11.37	19.75	14.18	15.25	18.06	19.1	26.34	1.111
57	21.74523	39.14492	1.487	2.88	6.27	13.77	25.83	16.56	17.37	19.89	20.92	35.05	1.176
58	21.74319	39.15473	1.333	2.332	6.27	10.01	20.6	13.18	14.28	17.05	18.32	22	1.25
59	21.74319	39.16424	11.05	1.546	6.44	8.705	15.37	12.05	13.3	16.16	17.51	18.54	13.333
60	21.74339	39.17398	0.763	1.7	5.4	3.379	9.927	10.58	12.32	15.59	16.51	17.69	13.333
61	21.74311	39.18352	1.28	4.149	5.98	12.39	22.8	14.83	16.31	19.3	19.74	29.37	1.176
62	21.74102	39.19562	2.09	2.325	6.09	9.237	18.45	12.51	13.81	16.99	17.56	19.17	1.818
63	21.73147	39.11798	1.167	2.59	6.75	9.248	15.31	12.21	13.43	16.2	17.68	18.93	14.286
64	21.73481	39.12047	1.24	2.828	7.07	9.78	17.01	12.59	13.81	16.66	17.85	20.3	1.176
65	21.73232	39.1261	1.342	2.2	6.96	8.641	15.07	11.73	12.99	15.86	17.17	18.63	14.286
66	21.73398	39.13536	1.28	2.615	6.97	9.408	16.41	12.25	13.48	16.42	17.72	19.18	1.25
67	21.73816	39.14192	1.504	3.46	4.96	11.36	24.97	14.43	15.25	18	19.18	26.78	1.333
68	21.73472	39.14508	1.52	4.413	5.22	13.59	31.91	16.47	17.2	19.69	20.73	34.14	1.333
69	21.73463	39.15477	1.297	2.74	4.97	9.605	17.29	12.64	13.82	16.77	17.96	20.61	1.25
70	21.7342	39.16447	1.461	1.59	4.96	7.424	12.13	10.81	12.27	15.36	16.69	17.86	13.333
71	21.73437	39.17376	3.65	1.611	5.52	8.029	13.29	15.56	13.18	15.68	17.21	18.21	13.333
72	21.72473	39.11737	1.048	3.24	6.65	10.34	16.4	13.16	14.32	17.29	18.51	22.13	1
73	21.72552	39.12577	1.24	2.58	6.24	9.288	15.75	12.28	13.49	16.46	17.87	19.04	14.286

Table 2 (*continued*)

Site No.	Lat.	Long.	F_0	A_0	PGA (bedrock)	PGA (surface)	PGA (1.5 Hz)	PGA (3 Hz)	PGA (5 Hz)	PGA (8 Hz)	PGA (10 Hz)	Max. PSA	Max. Hz
74	21.72467	39.13529	1.352	5.13	6.36	14.67	30.11	17.2	18.03	20.53	21.64	37.54	1.176
75	21.72471	39.14556	1.48	4.503	6.75	13.7	31.35	16.43	17.14	19.5	20.74	33.9	1.429
76	21.71603	39.11357	1.013	1.33	7.17	7.338	9.57	10.82	12.28	15.49	16.89	18.27	12.5

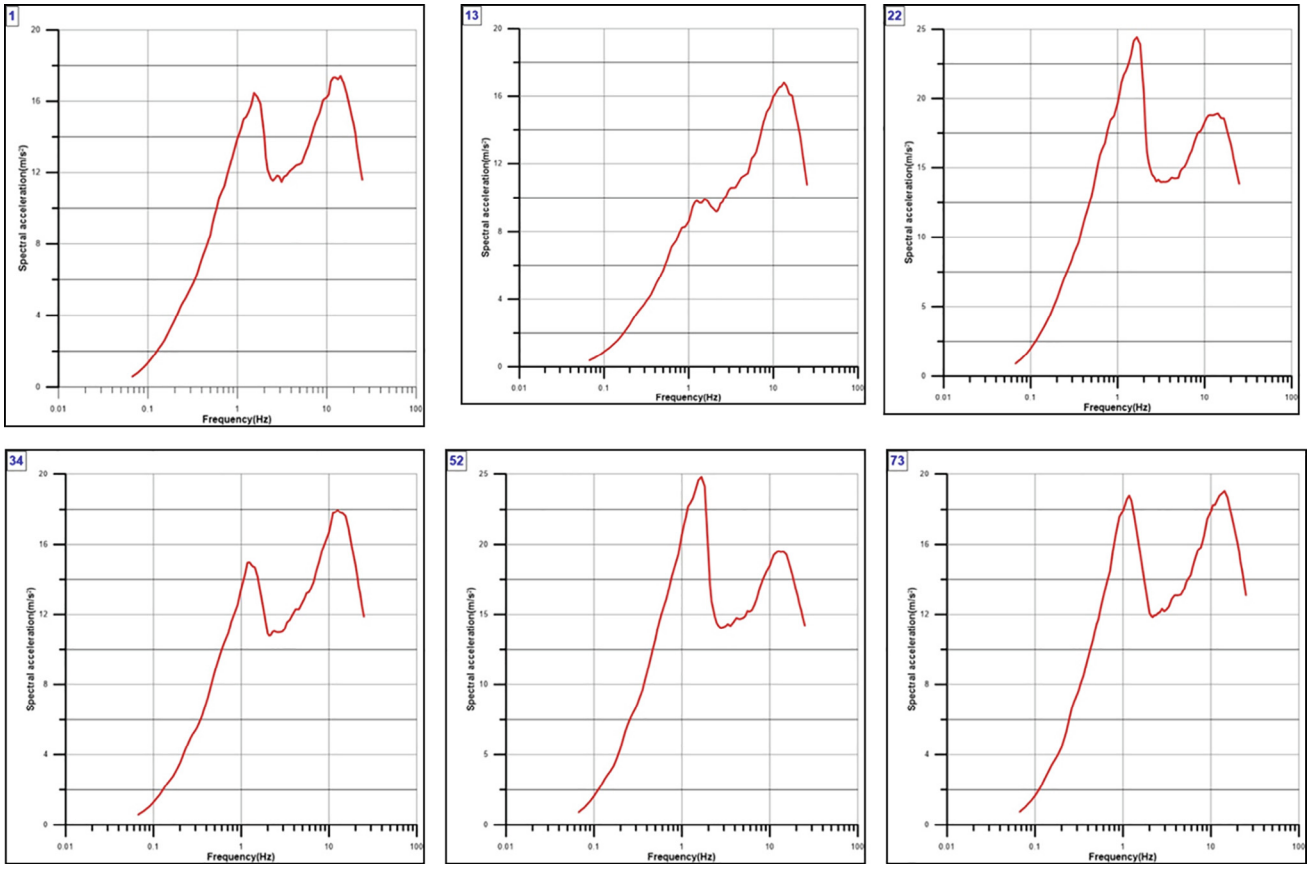

Fig. 5. Ground response spectra for 5% damping at MASW sites in the study area.

recorded depth of engineering bedrock for northern Jeddah urban area varies from zero (exposed on the ground surface) to approximately 36.23 m below ground surface. This depth in the western part is less than 15 m while increased eastward where it ranges between 20 and 36 m depth. This indicates that the engineering bedrock in the western zone obtained at a shallow depth than the rest of the studied area. These results correlated with the borehole data of Aldahri et al. (2017).

The ground motion frequency is of utmost importance where the *PGA* value alone cannot describe the surface ground motion. So, the response spectra are widely accepted parameter to specify the frequency content. Accordingly, the integrated influences of acceleration, amplitude, and frequency components can be expressed well the effects of ground motion. In this study, the ground surface response spectra for 76 locations were plotted with 5% critical damping. Fig. 5 shows examples of ground response analysis at the MASW site Nos. 1, 13, 22, 34, 52, and 73. Site No. 1 presents two PGA peaks of 16.53 cm/s^2 and 17.64 cm/s^2 which occurred at 1.25 Hz and 10.37 Hz, respectively. Site No. 13 shows two PGA peaks of 9.9 cm/s^2 and 17.0 cm/s^2 at 1.5 Hz and 10.7 Hz, respectively. Furthermore, site No. 22 shows two PGA peaks of 24.6 cm/s^2 and 18.3 cm/s^2 at 2.0 Hz and 10.5 Hz, respectively. Moreover, site No. 34 shows two PGA peaks of 15.5 cm/s^2 and 17.9 cm/s^2 at 1.53 Hz and 10.6 Hz, respectively. In addition, site No. 52 shows two PGA peaks of 24.9 cm/s^2 and 19.5 cm/s^2 at 2.0 Hz and 10.75 Hz, respectively. Finally, site No. 73 shows two PGA peaks with the same value of 18.5 cm/s^2 at 1.3 Hz and 10.9 Hz. According to these values, it can be stated that there is vertical variation in the density of the subsurface materials where these sediments vary from dense to very dense at different depths which is reflected in the presence of two fundamental resonance frequencies at the MASW measurement sites.

The spectral acceleration (*SA*) values for all MASW stations of measurements at 1.5, 3, 5, 8, and 10 Hz were computed. These frequencies represent the frequency range for single-story to multi-story buildings (Day, 2001). The Peak spectral acceleration (PSA) and corresponding frequency of each site were calculated. PSA varies from 16.8 to 62.6 cm/s^2 (Fig. 6). The eastern study area has higher spectral acceleration compared to the western part. Table 2 shows that the frequency corresponding to the *PSA* varies from 1.05 to 14.28 *Hz*.

Most of the urban area characterized by low-rise buildings and the frequency of the soil cover can be close to their fundamental

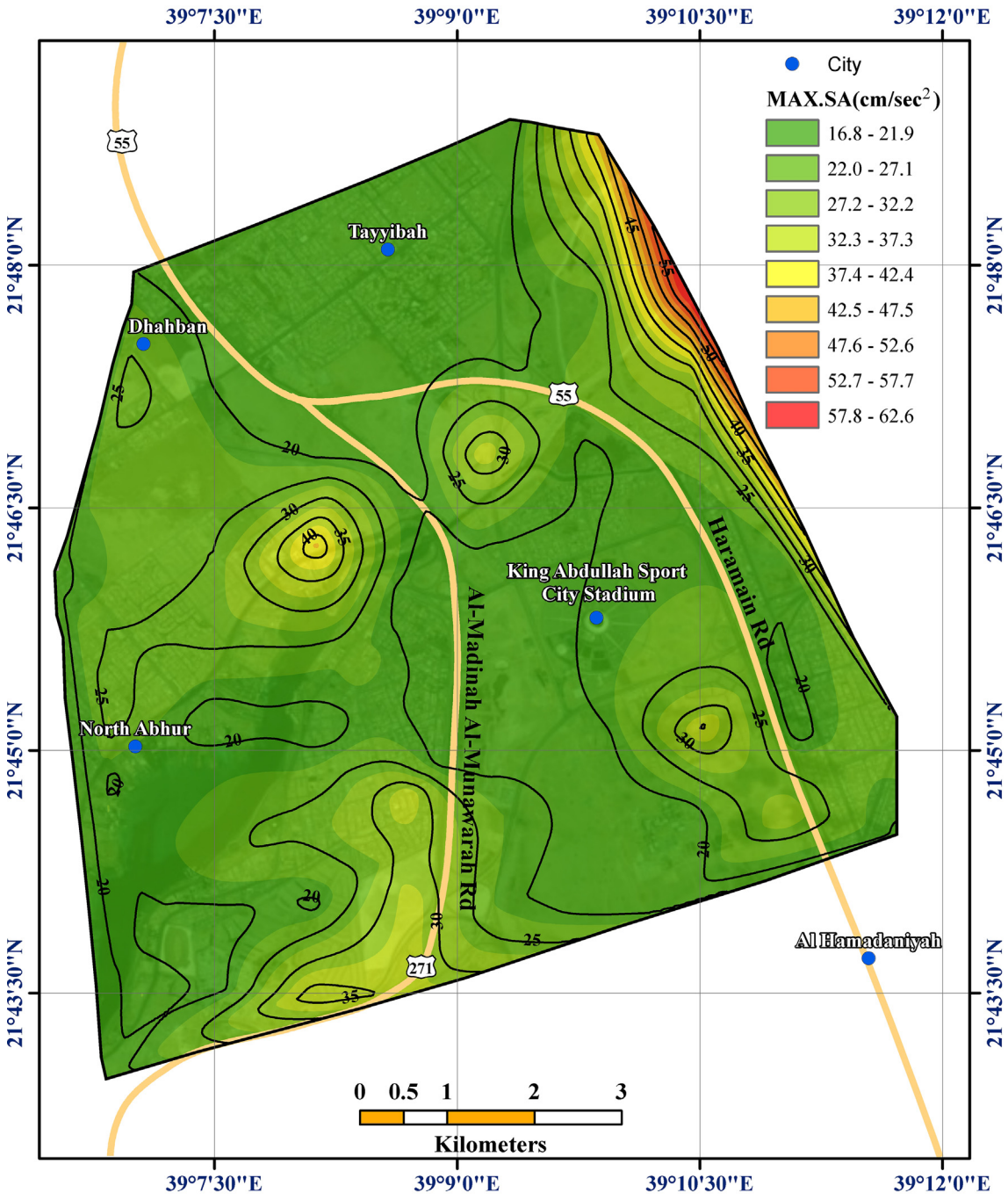

Fig. 6. Maximum peak spectral ground acceleration with 5% damping at the study area.

frequency of vibration. According to Parolai et al., (2006), when the fundamental frequency of vibration of a building is higher than that the fundamental frequency of soil fo it may, however be, close to the frequency of higher modes. Higher modes are expected at frequencies fn = (2n + 1) f_o where n = 1,2,3. . .. . . and f_o is the fundamental frequency. The H/V spectral ratio provides the lower frequency threshold from which ground motion amplification due to soft soil can be expected (Aldahri et al., 2018). Therefore, it cannot exclude that in the study area, such soil amplification of ground motions may occur at higher mode frequencies close to the fundamental frequency of vibration of low-rise buildings, even if it is smaller than that at the fundamental frequency of the sedimentary cover (Parolai et al., 2006).

5. Conclusions

Based on the aforementioned, it is highly recommended that the sites of unconsolidated sediments should be treated from an engineering perspective. Although the value of the spectral acceleration is not high, it may be hazardous where the risk lies in the value of the frequency corresponding to the spectral acceleration, which may cause severe damage to facilities and infrastructure. This point should be considered before designing important engineering facilities in the study area. Results of this study should be forwarded to civil engineers, land-used planners, and decision makers during the design of either new buildings or rehabilitation of pre-existing structures.

Declaration of Competing Interest

The authors declare that they have no known competing financial interests or personal relationships that could have appeared to influence the work reported in this paper.

Acknowledgments

The authors extend their appreciation to the Deanship of Scientific Research at King Saud University for funding this work through research group No. (RG-1440-003). Great thanks are extending to the reviewers for their beneficial review and valuable comments.

References

Aldahri, M., El-Hadidy, M., Zahran, H., Hassanein, K.A., 2018. Seismic microzonation of Ubhur district, Jeddah, Saudi Arabia, using H/V spectral ratio. Arab. J. Geosci. 11 (6). https://doi.org/10.1007/s12517-018-3415-8.

Aldahri, M., Mogren, S., Abdelrahman, K., Zahran, H., El Hady, Sh., El-Hadidy, M., 2017. Surface soil assessment in the Ubhur area, north of Jeddah, western Saudi Arabia, using a multichannel analysis of surface waves method. J. Geol. Soc. India 89, 435–443.

Akin, M., Kramer, S., Topal, T., 2013. Evaluation of Site Amplification of Erbaa, Tokat (Turkey). Seventh International Conference on Case Histories in Geotechnical Engineering. Paper 23. http://scholarsmine.mst.edu/icchge/7icchge/session04/23..

Ambraseys, N., Melville, C., Adams, R., 1994. The Seismicity of Egypt, Arabia and the Red Sea: A Historical Review. Cambridge University Press, UK, p. 181.

Ansal, A., Tonuk, G., 2007. Source and site factors in microzonation. In: Pitilakis, K.D. (Ed.), Earthquake Geotechnical Engineering, 4th International Conference on Earthquake Geotechnical Engineering-Invited Lectures, pp. 73–92..

Boore, D.M., 1983. Stochastic simulation of high-frequency ground motions based on seismological models of the radiated spectra. Bull. Seism. Soc. Am. 73, 1865–1894.

Boore, D.M., 2003. Simulation of ground motion using the stochastic method. Pure Appl. Geophys. 160, 635–675.

Boore, D.M., 2004. Estimating Vs30 (or NEHRP site Classes) from shallow velocity models (depths < 30 m). BSSA 94, 591–597.

Boore, D.M., Joyner, W.B., 1997. Site amplifications for generic rock sites. Bull. Seism. Soc. Am. 87, 327–341.

Brune, J., 1970. Tectonic stress and the spectra of seismic shear waves from earthquakes. J. Geophys. Res. 75 (26), 4997–5009.

Day, R.W., 2001. Geotechnical Earthquake Engineering Handbook. McGraw-Hill.

Fnais, M.S., Abdel-Rahman, K., Al-Amri, A.M., 2010. Microtremor measurements in Yanbu City of western Saudi Arabia: a tool of seismic microzonation. J. King Saud University-Science 22, 97–110. https://doi.org/10.1016/j.jksus.2010.02.006.

Hanks, T.C., Kanamori, H., 1979. A moment magnitude scale. J. Geophys. Res. 84 (B5), 2348. https://doi.org/10.1029/JB084iB05p02348.

Kanli, A.I., Tildy, P., Pronay, Z., Pinar, A., Hemann, L., 2006. Vs30 mapping and soil classification for seismic site effect evaluation in Dinar region, SW Turkey. Geophys. J. Int. 165, 223–235.

Kanlı, A.I., 2010. Integrated Approach for Surface Wave Analysis from Near-Surface to Bedrock, Chapter 29, p. 461–476, Advances in Near-Surface Seismology, Geophysical Developments Series No. 15, SEG Reference Publications, Society of Exploration Geophysics Reference Publications Program, Tulsa, Oklahoma-USA. Publisher: Society of Exploration Geophysicists, American Geophysical Union and Environmental and Engineering Geophysical Society (Ed. Com.: R.D. Miller, J.D. Bradford and K. Holliger)..

Moore, T.A., Al-Rehaili, M.H., 1989. Geologic Map of the Makkah Quadrangle, Sheet 21D, Kingdom of Saudi Arabia, Ministry of Petroleum and Mineral Resources, Deputy Ministry for Mineral Resources Publication, Jeddah, K.S.A..

Miller, R.D., Xia, J., Park, C.B., Ivanov, J.M., 1999. Multichannel Analysis of Surface Waves to Map Bedrock. Kansas Geological Survey, The Leading Edge, pp. 1392–1396.

Nath, S.K., 2007. Seismic microzonation framework-principles and applications, Proc. Workshop on Microzonation, Indian Institute of Science, Bangalore, 26 – 27 June 2007, India, pp. 9–35..

NEHRP, 2009. NEHRP recommended seismic provisions for new buildings and other structures (FEMA-P750). FEMA, Washington DC.

Park, C.B., Miller, R.D., Xia, J., 1999. Multichannel analysis of surface waves. Geophysics 64 (3), 800–808.

Park, C.B., Miller, R.D., 2005. Seismic characterization of wind turbine sites near Lawton, Oklahoma, by the MASW method: Kansas Geological Survey Open-file Report 2005-22..

Park, C.B., Ivanov, J., Miller, R.D., Xia, J., Ryden, N., 2001. Seismic investigation of pavements by MASW method-geophones approach, Proc. SAGEEP 2001, Denver, Colorado, RBA-6..

Parolai, S, Bormann, P., Milkereit, C., 2006. Measurements of the fundamental resonance frequency of the sedimentary cover in thje Cologne area: contribution to the seismic microzonation. Ergebnisse aus dem Deutschen Forschungesnetz Naturkatastrophen, pp. 301–305..

Rehman, F., Elnashar, Sh., Atef, A., Harbi, H., 2016. Multichannel analysis of surface waves for seismic site characterization using 2D genetic algorithm at Bahrah area, Wadi Fatima, Saudi Arabia. Arabian J. Geosci. 9 (8). https://doi.org/10.1007/s12517-016-2544-1.

Ryden, N., 2004. Surface Wave Testing of Pavements. Doctoral Thesis, Department of Engineering Geology. Lund Institute of Technology, Lund University.

Santamarina, J.C., Klein, K.A., Fam, M.A., 2001. Soil and Waves. John Wiley & Sons Inc, New York.

Sokolov, V., Zahran, H.M., 2018. Generation of stochastic earthquake ground motion in western Saudi Arabia as a first step in development of regional ground motion prediction model. Arabian J. Geosci. 11, 38.

Xia, J., Miller, R.D., Park, C.B., 1999. Estimation of near-surface shear-wave velocity by inversion of Rayleigh wave. Geophysics 64, 691–700.

Zhang, S.X., Chan, L.S., Xia, J., 2004. The selection of field acquisition parameters for dispersion images from multichannel surface wave data. Pure Appl. Geophys. 161, 185–201.